TECHNICAL PAPER

Particle focusing in a contactless dielectrophoretic microfluidic chip with insulating structures

Chun-Ping Jen · Nikolay A. Maslov ·
Hsin-Yuan Shih · Yung-Chun Lee · Fei-Bin Hsiao

Abstract The focusing of biological and synthetic particles in microfluidic devices is a crucial step for the construction of many microstructured materials as well as for medical applications. The present study examines the feasibility of using contactless dielectrophoresis (cDEP) in an insulator-based dielectrophoretic (iDEP) microdevice to effectively focus particles. Particles 10 μm in diameter were introduced into the microchannel and pre-confined hydrodynamically by funnel-shaped insulating structures near the inlet. The particles were repelled toward the center of the microchannel by the negative DEP forces generated by the insulating structures. The microchip was fabricated based on the concept of cDEP. The electric field in the main microchannel was generated using electrodes inserted into two conductive micro-reservoirs, which were separated from the main microchannel by 20-μm-thick insulating barriers made of polydimethylsiloxane (PDMS). The impedance spectrum of the thin insulating PDMS barrier was measured to investigate its capacitive behavior. Experiments employing polystyrene particles were conducted to demonstrate the feasibility of the proposed microdevice. Results show that the particle focusing performance increased with increasing frequency of the applied AC voltage due to the reduced impedance of PDMS barriers at high frequencies. When the frequency was above 800 kHz, most particles were focused into a single file. The smallest width of focused particles distributed at the outlet was about 13.1 μm at a frequency of 1 MHz. Experimental results also show that the particle focusing performance improved with increasing applied electric field strength and decreasing inlet flow rate. The usage of the cDEP technique makes the proposed microchip mechanically robust and chemically inert.

C.-P. Jen (✉)
Department of Mechanical Engineering,
Advanced Institute of Manufacturing with High-tech
Innovations, National Chung Cheng University,
Chia Yi, Taiwan, ROC
e-mail: imecpj@ccu.edu.tw

N. A. Maslov
Khristianovich Institute of Theoretical and Applied Mechanics,
Siberian Division, Russian Academy of Science,
Novosibirsk, Russia

H.-Y. Shih · F.-B. Hsiao
Institute of Aeronautics and Astronautics, National Cheng Kung
University, Tainan, Taiwan, ROC

Y.-C. Lee
Department of Mechanical Engineering, National Cheng Kung
University, Tainan, Taiwan, ROC

1 Introduction

The focusing of biological and synthetic particles in microfluidic devices is a crucial step for the construction of many microstructured materials, including biomaterials such as tissues and biofilms (Flores-Rodriguez and Markx 2006), as well as for medical applications, such as cell sorting, counting, and flow cytometry (Mostert et al. 2009). Numerous methods of particle focusing have been proposed (Xuan et al. 2010). Focusing by sheath flow (Howell Jr. et al. 2008; Watkins et al. 2009; Lee et al. 2009) is a widely employed method for particle focusing; however, additional buffer inlets and precise flow control are needed. Sheathless focusing, which relies on either an externally applied or an internally induced force field, has also been investigated (Xuan et al. 2010). Dielectrophoresis (DEP), which is achieved under a non-uniform electric field generated by various electrode patterns, insulating structures,

or their combination, has been widely used for the manipulation of cells in various microdevices. Dielectrophoresis produces a contact-free force, which makes it particularly suitable for cell manipulation in a microchip. Early studies on DEP response adopted large electrodes, such as needles, pins, wires, or sheets (Pohl 1978; Jones and Kraybill 1986). Microfabrication technology was later employed to create microelectrode patterns, enabling sufficiently large DEP forces to be generated to manipulate particles with the application of small voltages. The direction of the DEP force is controlled by the dielectric properties of the particles and medium, which are functions of frequency. Microelectrode patterns used for DEP have been previously reviewed (Ramos et al. 1998; Voldman 2006). Geometrical constrictions in insulating structures have also been proposed to produce non-uniform electric fields by squeezing the electric field in a conductive medium, termed insulator-based DEP (iDEP) (Lapizco-Encinas et al. 2004). Methods of particle focusing using DEP have been developed. Flores-Rodriguez and Markx (Flores-Rodriguez and Markx 2006) proposed a design in which non-uniform electric fields are generated between microelectrodes on the top and bottom of the microchannel, focusing particles along channels. The DEP confinement of particles generated by microelectrodes on the top and bottom of the channel has been employed to achieve particle focusing, detection, and counting (Holmes et al. 2006). A three-dimensional, particle-focusing channel that uses positive DEP guided by a dielectric structure between two planar electrodes has been reported (Chu et al. 2009). However, positive DEP is inappropriate for continuous manipulation due to particle adherence on the electrodes or regions with a high electric-field gradient in the microchannel. Particles in a microchannel have been accurately manipulated using DEP generated by an electric field between liquid electrodes (Demierre et al. 2007). An alternative technique, termed contactless dielectrophoresis (cDEP), has been proposed to provide the non-uniform electric fields in microfluidic channels required for the DEP manipulation of cells without direct contact between the electrodes and the sample (Shafiee et al. 2009). The electric field is created in the sample microchannel using electrodes inserted into two conductive microchambers which are separated from the sample channel by thin insulating barriers. Microfluidic devices capable of selectively isolating live human leukemia cells from dead cells utilizing their electrical signatures have been developed (Shafiee et al. 2010). The frequency response of breast cancer, leukemia, macrophages and red blood cells has also been investigated using the cDEP device (Sano et al. 2011). Hence, conditions to detect and enrich circulating tumor cells (CTCs) from a peripheral blood sample can be determined to develop methods to isolate these rare cells. Additionally,

the DEP response of prostate tumor initiating cells (TICs) has been observed to be distinctively different than that for non-TICs in a microfluidic system employing the technique of cDEP (Salmanzadeh et al. 2012). Therefore, the marker-free TIC separation from non-TICs utilizing their electrical signatures through DEP has been achieved. An iDEP microdevice that can sheathlessly focus HeLa cells in two directions was designed and demonstrated in our previous work (Jen et al. 2010a). The measured width of focused cells distributed at the outlet in our previous microdevice for two-dimensional focusing was approximately 39 μm with an applied voltage of 100 V and an inlet flow rate of 0.5 μL/min. In our previous study, the metallic electrodes were deposited on a glass substrate to reduce the required applied voltage; however, the electrodes were exposed to the medium solution, which resulted in electrolysis during experiments. The present study examines the feasibility of applying cDEP to our design of an insulator-based DEP microdevice to effectively focus particles. Furthermore, the frequency-dependent impedance of thin insulating barriers is measured to optimize the operating frequency.

2 Theory

The DEP force (F_{DEP}) acting on a spherical particle of radius R suspended in a fluid with permittivity ε_m is given as

$$F_{DEP} = 2\pi R^3 \varepsilon_m \mathrm{Re}(f_{CM})\nabla E_{rms}^2 \qquad (1)$$

where $\mathrm{Re}(f_{CM})$ is the real part of the Clausius–Mossotti factor and E_{rms} is the root-mean-square of the external electric field, in an alternating current (AC) field. The Clausius–Mossotti factor (f_{CM}) is a parameter of the effective polarizability of a particle. It varies with the complex dielectric properties of the particle and the surrounding medium, which are functions of the frequency of the applied field (f). The Clausius–Mossotti factor for a spherical particle is represented as

$$f_{CM} = \left[\frac{\varepsilon_p^* - \varepsilon_m^*}{\varepsilon_p^* + 2\varepsilon_m^*}\right] \qquad (2)$$

where ε_p* and ε_m* are the complex permittivities of the particle and the medium, respectively. The complex permittivity is related to the conductivity σ and angular frequency $\omega = 2\pi f$ as

$$\varepsilon^* \equiv \varepsilon - j\frac{\sigma}{\omega} \qquad (3)$$

where j equals $\sqrt{-1}$. Therefore, the DEP force depends mainly on the difference between the dielectric properties of the particles and those of the suspending medium solution. The DEP force can be either positive, pulling

particles toward the region with a high electric-field gradient, or negative, repelling particles away from the region with a high electric-field gradient.

A numerical simulation of the electric and flow fields as well as the particle trajectories was performed using the commercial software package CFD-ACE$^+$ (ESI Group, France). The finite element method and two-dimensional structured grids were employed to solve the governing equations. The governing equations for the flow field in this study are the continuity and momentum conservation (Navier–Stokes) equations. The dimensionless forms can be expressed as

$$\nabla^* V^* = 0 \tag{4}$$

$$\frac{dV^*}{dt^*} = -\nabla^* P^* + \frac{1}{\text{Re}} \nabla^{*2} V^* \tag{5}$$

where $\text{Re} = \frac{\rho U D_h}{\mu}$, in which D_h and U are the hydraulic diameter of the microchannel and inlet velocity of the fluid, respectively. P^* is the dimensionless pressure and V^* is the dimensionless velocity vector. ρ and μ are the density and dynamic viscosity of the medium, respectively. The governing equation for the electric potential ϕ in the medium can be expressed as

$$\nabla \cdot \left[\sigma_m \nabla \varphi + \varepsilon_m \frac{\partial \nabla \varphi}{\partial t} \right] = 0 \tag{6}$$

where σ_m and ε_m are the conductivity and permittivity of the medium, respectively. The current continuity equation is solved by assuming a sinusoidal steady state. After converting the current continuity equation into the frequency domain, where the electric potential becomes a complex quantity, the following equation is obtained

$$\nabla \cdot [\sigma_m + j\omega\varepsilon_m]\nabla \varphi = 0 \tag{7}$$

Since the electric potential of the above equation is complex, that is, $\phi = \phi_r + j\phi_i$ the following two equations must be solved

$$\nabla \cdot \sigma_m \nabla \varphi_i + \nabla \cdot \omega\varepsilon_m \nabla \varphi_r = 0 \tag{8}$$

$$\nabla \cdot \sigma_m \nabla \varphi_r - \nabla \cdot \omega\varepsilon_m \nabla \varphi_i = 0 \tag{9}$$

The electric field is assumed to be unaffected by the presence of particles in the simulation for simplicity. Discrete particles are tracked in the microchannel by solving the Lagrangian equations, taking into consideration both the DEP force and drag force in the simulation. The drag force acting on a particle is given by

$$F_D = \frac{1}{2} \rho U_r^2 A C_D \tag{10}$$

where U_r is the relative velocity of the fluid over a particle, and A is the projection area of a particle ($A = \pi R^2$). C_D is the drag coefficient of a particle from the particle drag

model of the CFD-ACE$^+$ tool. Particle–particle interactions are ignored in the simulation.

3 Experimental section

3.1 Device layout

A schematic diagram of the microfluidic chip is shown in Fig. 1. Four insulating structures, which formed an X-pattern in the microchannel, were employed to squeeze the electric field in a conducting solution, thereby generating high-electric-field regions. The structure of insulators, which are 60 μm wide, 200 μm long, and 100 μm high, was designed and optimized in our previous investigation (Jen et al. 2010b). Both the distances between individual insulators along and perpendicular to the flow (2D and 2S, respectively) are 120 μm, and the inclined angle of the insulators is 45 degrees. The minimum width at the constricting region (L_c in Fig. 1) is 60 μm. Particles are introduced into the microchannel and pre-confined hydrodynamically by the funnel-shaped insulating structures near the inlet. The particles flow into the constricting regions (high electric-field gradient regions) at the edges of the insulating structures. Particles with a negative DEP response are repelled toward the center of the constricting region and focused as they pass through.

3.2 Chip fabrication

A lower conductive material of polydimethylsiloxane (PDMS) was adopted as a structure for distorting the electric field in a conducting solution, thereby generating regions with a high electric-field gradient. The mold master was fabricated using the inductively coupled plasma (ICP) dry etching technique on a silicon wafer (around 100 μm in height) to define the micropatterns, as shown in Fig. 2a. A
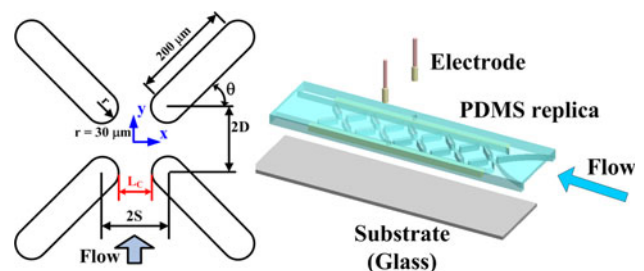
Fig. 1 Schematic illustration of the microfluidic chip for the DEP focusing of particles. Both the distances between individual insulators along and perpendicular to the flow (2D and 2S, respectively) are 120 μm, and the inclined angle of the insulators (θ) is 45 degrees. The minimum width at the constricting region (L_c) is 60 μm. Nine sets of X-patterned insulating structures were designed to generate non-uniform electric fields

releasing layer of 1H, 1H, 2H, 2H-perfluorooctyltri-chlorosilane with about 10 nm in thickness was then deposited on the silicon mold surface using the vapor deposition method (Jung et al. 2005; Lee and Chiu 2008). This releasing layer has good adhesion with the silicon substrate and been widely used for the anti-adhesion layer. Electrodes were inserted into two conductive micro-reservoirs, which were separated from the main microchannel (600 µm wide) by 20-µm-thick and 5.5-mm-long insulating PDMS barriers, to generate the electric field required for the DEP focusing. The PDMS prepolymer mixture (Sylgard-184 silicone elastomer kit, Dow Corning, Midland, MI, USA) was poured into the mold master coated with the releasing layer and cured to fabricate the structures. After the PDMS had been peeled off, the inlet and outlet ports were made by a puncher, and the replica with the patterned structures was bonded to the glass substrate, which was cleaned in piranha solution, after treatment with oxygen plasma in an O_2 plasma cleaner (Model PDC-32G, Harrick Plasma Corp., Ithaca, NY, USA). A photograph of the microchip taken by an optical microscope and a scanning electron microscopy (SEM) image of the PDMS replica are shown in Fig. 2b.

3.3 Apparatus and materials

A function/arbitrary waveform generator (Agilent 33220A, Agilent Technology, Palo Alto, CA, USA) was employed as the AC signal source. It was connected to an RF amplifier (HSA-4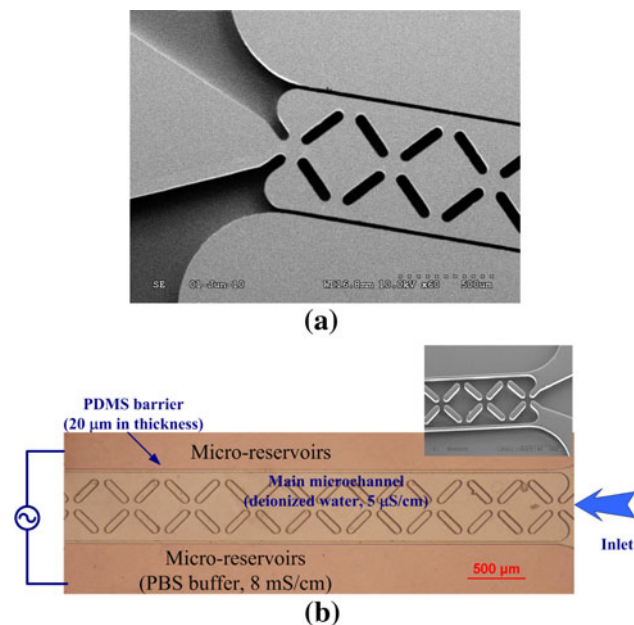011, NF Corporation, Japan) to apply the electric fields required for DEP focusing in the microchannel, and provides the required voltage (up to 160 V peak-to-peak at a frequency of 1 MHz). Polystyrene particles, 10 µm in diameter (G1000, Thermo Scientific Inc., USA) were used for the proof of concept demonstration and to investigate the efficiency of focusing. A sample of polystyrene particles with a concentration of 10^6 particles/mL was injected using a syringe pump (Model KDS 101, KD Scientific Inc., Holliston, MA, USA). The dielectric permittivity and conductivity of the polystyrene particles at a frequency of 1 MHz were about $2.6\varepsilon_0$ F/m and 10^{-16} S/m, respectively (Kang et al. 2009). The particles were suspended in deionized water ($\varepsilon = 78\varepsilon_0$ F/m; $\sigma = 5.0$ µS/cm), in which they exhibited a negative DEP response at a frequency of 1 MHz. The DEP focusing of particles was observed and recorded using an inverted fluorescence microscope (Model CKX41, Olympus, Tokyo, Japan), a mounted CCD camera (DP71, Olympus, Tokyo, Japan), and a computer running Olympus DP controller image software. Moreover, a precision impedance analyzer (Model 6420, Wayne Kerr Electronics Ltd., London, UK) was employed to measure the impedance spectrum of the thin insulating PDMS barrier to investigate its capacitive behavior.

4 Results and discussion

In order to understand the capacitive behavior of the thin insulating PDMS barrier, a chip comprising two micro-reservoirs separated by an insulating barrier was fabricated for the measurement of the impedance spectrum of the PDMS barrier. A schematic illustration of the experimental set up is shown in Fig. 3. The micro-reservoirs were filled with phosphate-buffered saline (PBS) buffer ($\varepsilon = 78\varepsilon_0$ F/m; $\sigma = 8.0$ mS/cm). The impedance spectrum of the PDMS was measured; results are shown in Fig. 4. The equivalent circuit model of the chip for measurement is shown in the inset of Fig. 4. The fitting curve to the experimental data was obtained using the least-squares method. The parameters in the equivalent circuit model were obtained as $R_{\text{liquid}} = 21.05$ kΩ, $R_{\text{PDMS}} = 224.15$ kΩ, and $C_{\text{PDMS}} =$
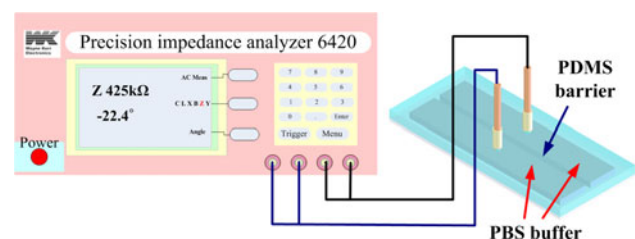

Fig. 2 **a** SEM micrograph of the mold on a silicon wafer, **b** photograph of the microchip and SEM micrograph of PDMS replica (*inset*)

Fig. 3 Schematic illustration of the experimental set up for measuring the impedance of the thin insulating PDMS barrier
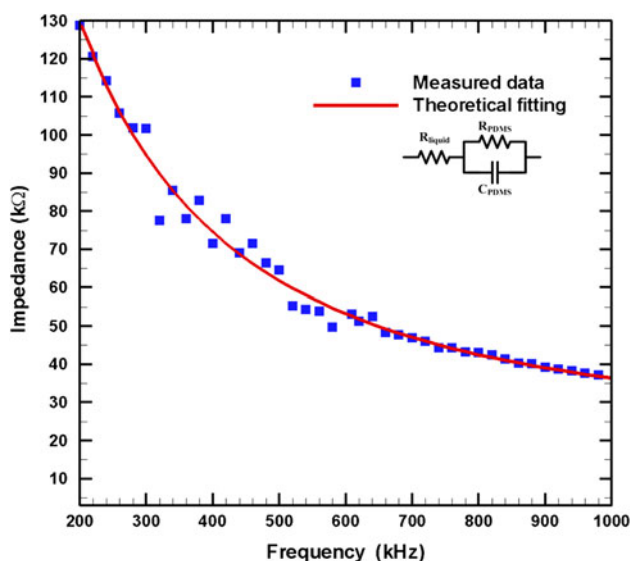
Fig. 4 Measured impedance of the thin insulating PDMS barrier under various frequencies and the fitting curve to experimental data obtained using the least-squares method. The equivalent circuit model of the chip for measurement is shown in the *inset*

5.80 μF. The spectrum indicates that the impedance of the PDMS decreased with increasing frequency. The impedance at 500 kHz is half of that at 200 kHz. When the frequency was 1 MHz, the impedance reduced to 37 kΩ. Assuming that the resistance of the liquid (R_{liquid}) is independent of frequency, the impedance of PDMS at 1 MHz is about 16 kΩ. Figure 5 shows the contours of ∇E^2 in the main microchannel with an applied voltage of 95 V peak-to-peak considering the impedance of the thin PDMS barriers at 1 MHz as well as the transient simulation of the tracks of negative DEP particles at an inlet flow rate of 2.0 μL/min. The simulation results indicate the locations of the high-electric-field regions. The particles were suspended in deionized water ($\varepsilon = 78\varepsilon_0$ F/m; $\sigma = 5.0$ μS/cm) and the electric field was constricted in the gap region between the insulating structures; thus, a strong highly non-uniform electric field was created near the edges of the insulating structures. The direction of the DEP force acting on the polystyrene particles is toward the center of the

microchannel. The DEP force acting on the negative DEP particles, which were distributed randomly at the inlet, is toward the local minima of the electric field, allowing particle focusing. To investigate the performance of focusing, polystyrene particles (10 μm in diameter) suspended in deionized water were prepared for experiments. Based on our previous results in simulation (Jen et al. 2010b), the performance of focusing reaches saturation while more than three sets of X-patterned insulating structures were designed in the microchannel. However, nine sets of X-patterned insulating structures were fabricated for particle focusing to ensure that the reliable experimental results could be obtained. Figure 6 shows the experimental results of particle focusing at various frequencies (from 100 kHz to 1 MHz) for an inlet flow rate and applied voltage of 0.5 μL/min and 160 V peak-to-peak, respectively. Photographs of the last two sets of X-patterned insulating structures (the region marked by the *dashed line* in the layout) were taken to demonstrate focusing performance. The widths of focused particles distributed at the outlet at various frequencies are indicated in the upper-left corner of each image. The particles randomly distributed throughout the microchannel without applying any electric field (data not shown); which implies that the effect of confinement by the funnel-shaped insulating structures only works near the inlet. The results indicate that the focusing performance increased with increasing frequency of the applied voltage due to the reduced impedance of PDMS barriers at high frequencies. The AC field generated by the electrodes at the microreservoirs generated an electric field in the main microchannel across the thin insulating barriers at high frequencies. Some particles were not focused and flowed to the sides of the microchannel when the frequency was below 800 kHz (Fig. 6a–d). The particles cannot be guided into the center of the microchannel once they flow to the sides of the channel at the beginning of X-patterned insulating structures. When the frequency was above 800 kHz (Fig. 6f), most particles were focused into a single file and the smallest width of focused particles distributed at the outlet was about 13.1 μm at a frequency of 1 MHz.
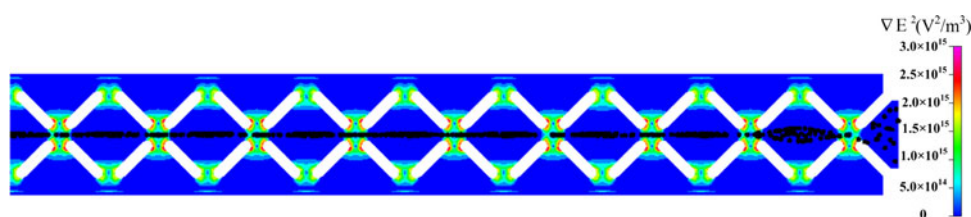

Fig. 5 Transient simulation of tracks of negative DEP particles and simulation results of the gradient of the square of the electric field (∇E^2) from a top view with an applied voltage of 95 V peak-to-peak and an inlet flow rate of 2.0 μL/min. The dielectric permittivity and conductivity of polystyrene particles at a frequency of 1 MHz were about $2.6\varepsilon_0$ F/m and 10^{-16} S/m, respectively. The particles were suspended in deionized water ($\varepsilon = 78\varepsilon_0$ F/m; $\sigma = 5.0$ μS/cm)
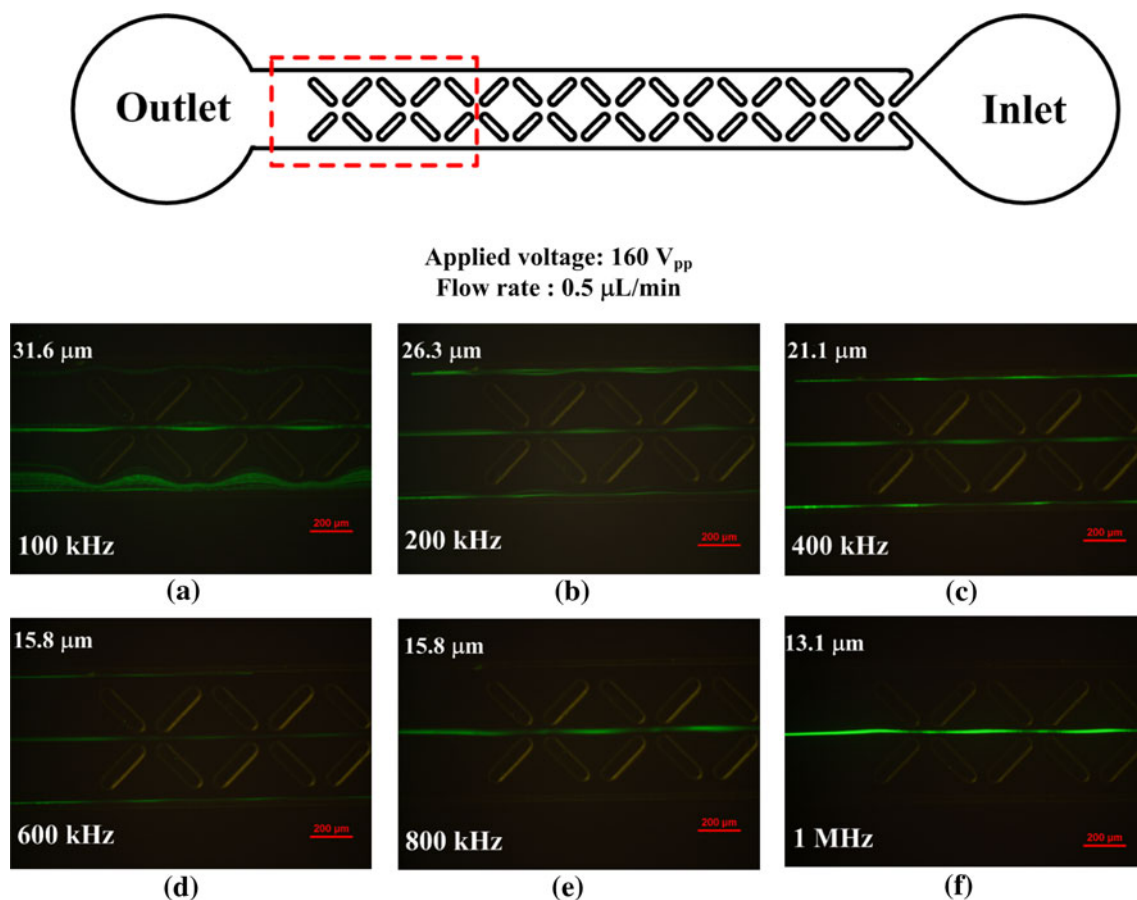
Fig. 6 Experimental results of focusing polystyrene particles at various frequencies at an applied voltage and inlet flow rate of 160 V peak-to-peak and 0.5 μL/min, respectively. Images of the last two sets of X-patterned insulating structures (the region marked by the *dashed line* in the layout) are shown to demonstrate the focusing performance. The widths of focused particles distributed at the outlet at various frequencies are indicated in the *upper-left corner* of each image

Figure 7 shows the experimental results of particle focusing at various inlet flow rates (0.5, 1.0, and 2.0 μL/min) and various applied voltages (95, 135, and 160 V peak-to-peak at 1 MHz). Experimental results show that the focusing performance improved with increasing applied electric field strength and decreasing inlet flow rate. The characteristic time scales due to the DEP and hydrodynamic forces are analyzed herein based on the method proposed by Salmanzadeh et al. (Salmanzadeh et al. 2011). The average of $\nabla(\vec{E}_{\text{rms}} \cdot \vec{E}_{\text{rms}})$ is on the order of 10^{14} V²/m³ (when a voltage of 95 V peak-to-peak was applied). The absolute value of the Clausius–Mossotti factor, Re(f_{CM}), for negative DEP is assumed as 0.5. Hence, the particle velocity due to the DEP force is about 150 μm/s. The characteristic distance for DEP is assumed as half of the channel width, i.e., $L_{\text{DEP}} = 300$ μm. The characteristic time for the DEP influence is $\tau_{\text{DEP}} \cong \frac{L_{\text{DEP}}}{u_{\text{DEP}}} \cong 2$ s. The minimum width at the constricting region (L_c in Fig. 1) is a tenth of the channel width. Thus, the characteristic velocity of the particle due to the flow (u_f) is assumed as tenfold of the average velocity in the channel, i.e., 3.93 mm/s, which is tenfold of a flow rate of 0.5 μL/min. The length of the microchannel (L_f) is approximately 5.5 mm. Accordingly, the characteristic residence time for the particle in the channel can be evaluated as $\tau_{\text{flow}} \cong \frac{L_f}{u_f} \cong 1.4$ s. The focusing of particles could be achieved while the characteristic residence time (τ_{flow}) is greater than, or comparable to that for the DEP influence (τ_{DEP}), as shown in Fig. 7a. When the applied voltage was 95 V, the particles were not focused when the flow rate was above 0.5 μL/min as shown in Fig. 7b, c. The criterion of focusing in the present study is defined as that the width of particles distributed at the outlet is smaller than the minimum width at the constricting region ($L_C = 60$μm). The characteristic residence time for the particle in the channel decreases while the inlet flow rate increases. The characteristic residence time is approximately 0.35 s (when the inlet flow rate is 2.0 μL/min), which is less than the characteristic time for the DEP influence ($\tau_{\text{DEP}} = 2$ s, when applying a voltage of 95 V peak-to-peak); hence, the performance of focusing is poor
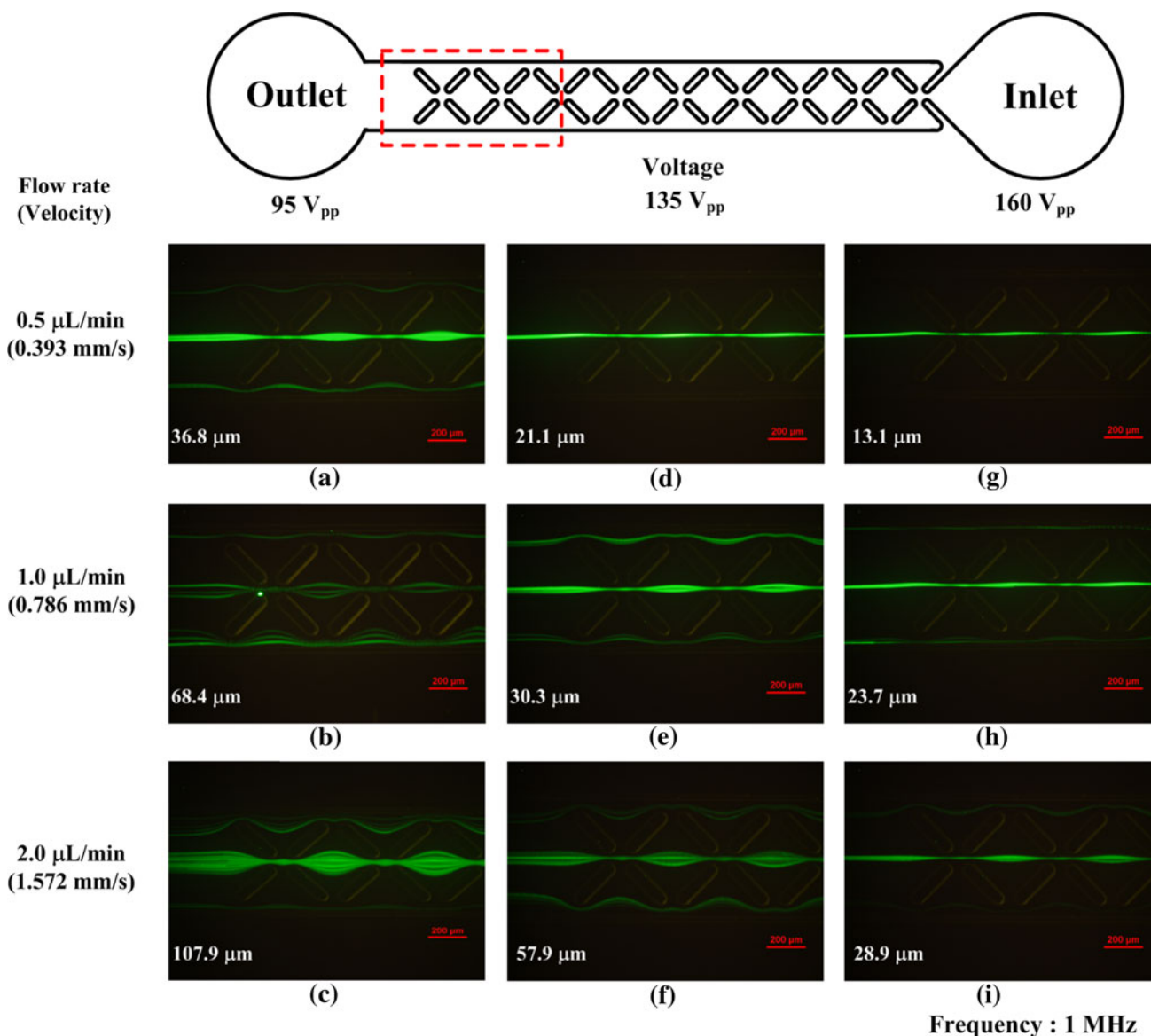
Fig. 7 Experimental results of particle focusing at various inlet flow rates and applied voltages (at a frequency of 1 MHz). Images of the last two sets of X-patterned insulating structures (the region marked by the *dashed line* in the layout) are shown to demonstrate the focusing performance. The widths of focused particles distributed at the outlet at various frequencies are indicated in the *upper-left corner* of each image

(Fig. 7c). A higher voltage applied implies the shorter characteristic time required for the DEP influence. When the applied voltage was increased to 135 V and the inlet flow rate was 0.5 μL/min (Fig. 7d), the particles were focused well at the center of the microchannel. The focusing of particles was achieved for all inlet flow rates for an applied voltage of 160 V (Fig. 7g–i), although some of the particles flowed to the sides of the microchannel at an inlet flow rate above 1.0 μL/min (Fig. 7i). The experimental results demonstrate the feasibility of applying cDEP to an insulator-based DEP microdevice to effectively focus particles.

5 Conclusion

Contactless dielectrophoresis was applied to an insulator-based DEP microdevice to effectively focus particles. Nine sets of X-patterned insulating structures were fabricated to squeeze the electric field in a conducting solution, thereby generating high-electric-field regions. The DEP force was employed to confine the particles with negative DEP responses. Experiments with polystyrene particles (10 μm in diameter) were conducted to demonstrate the feasibility of the proposed microdevice. Experimental results show that the focusing performance increased with increasing

frequency of the applied AC voltage due to the reduced impedance of PDMS barriers at high frequencies. When the frequency was above 800 kHz, most particles were focused into a single file and the smallest width of focused particles distributed at the outlet was about 13.1 μm at a frequency of 1 MHz. Experimental results also show that the focusing performance improved with increasing applied electric field strength and decreasing inlet flow rate. The usage of cDEP technique makes the proposed microdevice mechanically robust and chemically inert. The microdevice is easy to operate and can be integrated with other biomedical applications, making it a very useful tool in the fields of biomedicine, chemistry, and particle science. However, cDEP relies on the application of a high-frequency AC electric signal to the electrodes, which are capacitively coupled to a microfluidic channel. Bioparticles, for example mammalian cells, may exhibit positive DEP in the range of frequency adopted herein and be trapped at the edges of the insulating structures. The use of a high-frequency AC electric signal limits the application of cDEP. This limitation may be overcome by adjusting the conductivity of the buffer medium or using alternative polymeric materials with low impedance at low frequencies in place of PDMS.

References

Chu H, Doh I, Cho Y (2009) A three-dimensional (3D) particle focusing channel using the positive dielectrophoresis (pDEP) guided by a dielectric structure between two planar electrodes. Lab Chip 9:686–691

Demierre N, Braschler T, Linderholm P, Seger U, van Lintel H, Renaud P (2007) Characterization and optimization of liquid electrodes for lateral dielectrophoresis. Lab Chip 7:355–365

Flores-Rodriguez N, Markx GH (2006) Flow-through devices for the ac electrokinetic construction of microstructured materials. J Micromech Microeng 16:349–355

Holmes D, Morgan H, Green NG (2006) High throughput particle analysis: combining dielectrophoretic particle focusing with confocal optical detection. Biosens Bioelectron 21:1621–1630

Howell PB Jr, Golden JP, Hilliard LR, Erickson JS, Mott DR, Ligler FS (2008) Two simple and rugged designs for creating microfluidic sheath flow. Lab Chip 8:1097–1103

Jen CP, Huang CT, Shih HY (2010a) Hydrodynamic separation of cells utilizing insulator-based dielectrophoresis. Microsyst Technol 16:1097–1104

Jen CP, Huang CT, Weng CH (2010b) Focusing of biological cells utilizing negative dielectrophoretic force generated by insulating structures. Microelec Eng 87:773–777

Jones TB, Kraybill JP (1986) Active feedback-controlled dielectrophoretic levitation. J Appl Phys 60:1247–1252

Jung GY, Li Z, Wu W, Chen Y, Olynick DL, Wang SY, Tong WM, Williams RS (2005) Vapor-phase self-assembled monolayer for improved mold release in nanoimprint lithography. Langmuir 21:1158–1161

Kang Y, Cetin B, Wu Z, Li D (2009) Continuous particle separation with localized AC-dielectrophoresis using embedded electrodes and an insulating hurdle. Electrochim Acta 54:1715–1720

Lapizco-Encinas BH, Simmons BA, Cummings EB, Fintschenko Y (2004) Dielectrophoretic concentration and separation of live and dead bacteria in an array of insulators. Anal Chem 76:1571–1579

Lee YC, Chiu CY (2008) Micro-/nano-lithography based on the contact transfer of thin film and mask embedded etching. J Micromech Microeng 18:075013

Lee MG, Choi S, Park JK (2009) Three-dimensional hydrodynamic focusing with a single sheath flow in a single-layer microfluidic device. Lab Chip 9:3155–3160

Mostert B, Sleijfer S, Foekens JA, Gratama JW (2009) Circulating tumor cells (CTCs): detection methods and their clinical relevance in breast cancer. Cancer Treat Rev 35:463–474

Pohl HA (1978) Dielectrophoresis. Cambridge University Press, NY

Ramos A, Morgan H, Green GN, Castellanos A (1998) Ac electrokinetics: a review of forces in microelectrode structures. J Phys D Appl Phys 31:2338–2353

Salmanzadeh A, Shafiee H, Davalos RV, Stremler MA (2011) Microfluidic mixing using contactless dielectrophoresis. Electrophoresis 32:2569–2578

Salmanzadeh A, Romero L, Shafiee H, Gallo-Villanueva RC, Stremler MA, Cramer SD, Davalos RV (2012) Isolation of prostate tumor initiating cells (TICs) through their dielectrophoretic signature. Lab Chip 12:182–189

Sano MB, Henslee EA, Schmelz E, Davalos RV (2011) Contactless dielectrophoretic spectroscopy: examination of the dielectric properties of cells found in blood. Electrophoresis 32:3164–3171

Shafiee H, Caldwell JL, Sano MB, Davalos RV (2009) Contactless dielectrophoresis: a new technique for cell manipulation. Biomed Microdevices 11:997–1006

Shafiee H, Sano MB, Henslee EA, Caldwell JL, Davalos RV (2010) Selective isolation of live/dead cells using contactless dielectrophoresis (cDEP). Lab Chip 10:438–445

Voldman J (2006) Electrical forces for microscale cell manipulation. Annu Rev Biomed Eng 8:425–454

Watkins N, Venkatesan BM, Toner M, Rodriguez W, Bashir R (2009) A robust electrical microcytometer with 3-dimensional hydrofocusing. Lab Chip 9:3177–3184

Xuan X, Zhu J, Church C (2010) Particle focusing in microfluidic devices. Microfluid Nanofluid 9:1–16